Bioactive Materials 22 (2023) 47–59

Contents lists available at ScienceDirect

Bioactive Materials

journal homepage: www.keaipublishing.com/en/journals/bioactive-materials

An enzyme-responsive and transformable PD-L1 blocking peptide-photosensitizer conjugate enables efficient photothermal immunotherapy for breast cancer

Yanan Sun [a,b,1], Bochen Lyu [a,1], Chang Yang [a], Bing He [a], Hua Zhang [a], Xueqing Wang [a,**], Qiang Zhang [a,*], Wenbing Dai [a,***]

[a] Beijing Key Laboratory of Molecular Pharmaceutics and New Drug Delivery Systems, State Key Laboratory of Natural and Biomimetic Drugs, School of Pharmaceutical Sciences, Peking University, Beijing, 100191, China

[b] Department of Pharmaceutics, School of Pharmaceutical Sciences, Hebei Medical University, Shijiazhuang, 050017, China

ARTICLE INFO

Keywords:
Transformable nanomedicine
Self-assembled peptide
Immune checkpoint blockade
Photothermal therapy
Photoimmunotherapy

ABSTRACT

Mild photothermal therapy combined with immune checkpoint blockade has received increasing attention for the treatment of advanced or metastatic cancers due to its good therapeutic efficacy. However, it remains a challenge to facilely integrate the two therapies and make it potential for clinical translation. This work designed a peptide-photosensitizer conjugate (PPC), which consisted of a PD-L1 antagonist peptide (CVRARTR), an MMP-2 specific cleavable sequence, a self-assembling motif, and the photosensitizer Purpurin 18. The single-component PPC can self-assemble into nanospheres which is suitable for intravenous injection. The PPC nanosphere is cleaved by MMP-2 when it accumulates in tumor sites, thereby initiating the cancer-specific release of the antagonist peptide. Simultaneously, the nanospheres gradually transform into co-assembled nanofibers, which promotes the retention of the remaining parts within the tumor. In vivo studies demonstrated that PPC nanospheres under laser irradiation promote the infiltration of cytotoxic T lymphocytes and maturation of DCs, which sensitize 4T1 tumor cells to immune checkpoint blockade therapy. Therefore, PPC nanospheres inhibit tumor growth efficiently both in situ and distally and blocked the formation of lung metastases. The present study provides a simple and efficient integrated strategy for breast cancer photoimmunotherapy.

1. Introduction

According to the World Health Organization, breast cancer remains a disease with high morbidity and mortality among women due to its complexity and metastatic potential [1]. Immunotherapy differs from traditional treatment methods because it has fewer side effects and is not likely to relapse after recovery [2,3]. Immune checkpoint blockade (ICB) blocks immunosuppressive signals in a tumor microenvironment and restores the function of cytotoxic T lymphocytes (CTLs) and has achieved good efficacy in breast cancer treatment [4,5]. However, clinical studies have shown that the therapeutic response for ICB alone is relatively low (~20%) due mainly to the different degrees of tumor-infiltrating lymphocytes and the expression of immunosuppressive molecules (e.g., PD-L1) in tumors [6,7]. Because of its lower-than-expected response, ICB is currently used in combination with other therapies (radiotherapy, chemotherapy, hyperthermia, and so on) to improve the immunogenicity of the tumor microenvironment and thus, enhance the response rate [8–10]. Currently, most of the drugs on the market that acts on the PD-1 or CTLA-4 signaling pathways are antibodies [4]. However, the antibody preparation process is complicated and expensive. In addition, the immunogenicity of macromolecular antibodies and other immunotherapy-associated side effects during systemic administration also limits their clinical applications [11,12].

Photothermal therapy (PTT), which utilizes a photosensitizer to

Peer review under responsibility of KeAi Communications Co., Ltd.

* Corresponding author.
** Corresponding author.
*** Corresponding author.
E-mail addresses: wangxq@bjmu.edu.cn (X. Wang), zqdodo@bjmu.edu.cn (Q. Zhang), daiwb@bjmu.edu.cn (W. Dai).

[1] These authors contributed equally to this work.

https://doi.org/10.1016/j.bioactmat.2022.08.020
Received 1 June 2022; Received in revised form 2 August 2022; Accepted 15 August 2022

2452-199X/© 2022 The Authors. Publishing services by Elsevier B.V. on behalf of KeAi Communications Co. Ltd. This is an open access article under the CC BY-NC-ND license (http://creativecommons.org/licenses/by-nc-nd/4.0/).

generate hyperthermia at the tumor site, has emerged as a promising strategy for cancer therapy. The advantages of PTT include low invasiveness and high efficacy [13]. Compared with the current photothermal ablation therapies (local temperature >50 °C), which potentially induce thermal damage and tumor metastasis, mild PTT with a lower local temperature (42–45 °C) incurs less damage to normal tissues surrounding the tumor [14]. Moreover, mild PTT can modulate the tumor microenvironment in several ways (i.e., by inducing immunogenic death of tumor cells [15], promoting immune cell infiltration into tumors [16]; promoting the maturation and migration of DCs to the draining lymph nodes [17], and enhancing the expression of PD-L1 in tumor cells), thereby enhancing their response to ICB therapy [18,19]. However, mild PTT has a limited ability to eradicate primary tumor cells [20], and the immune remodeling that is induced is relatively weak and

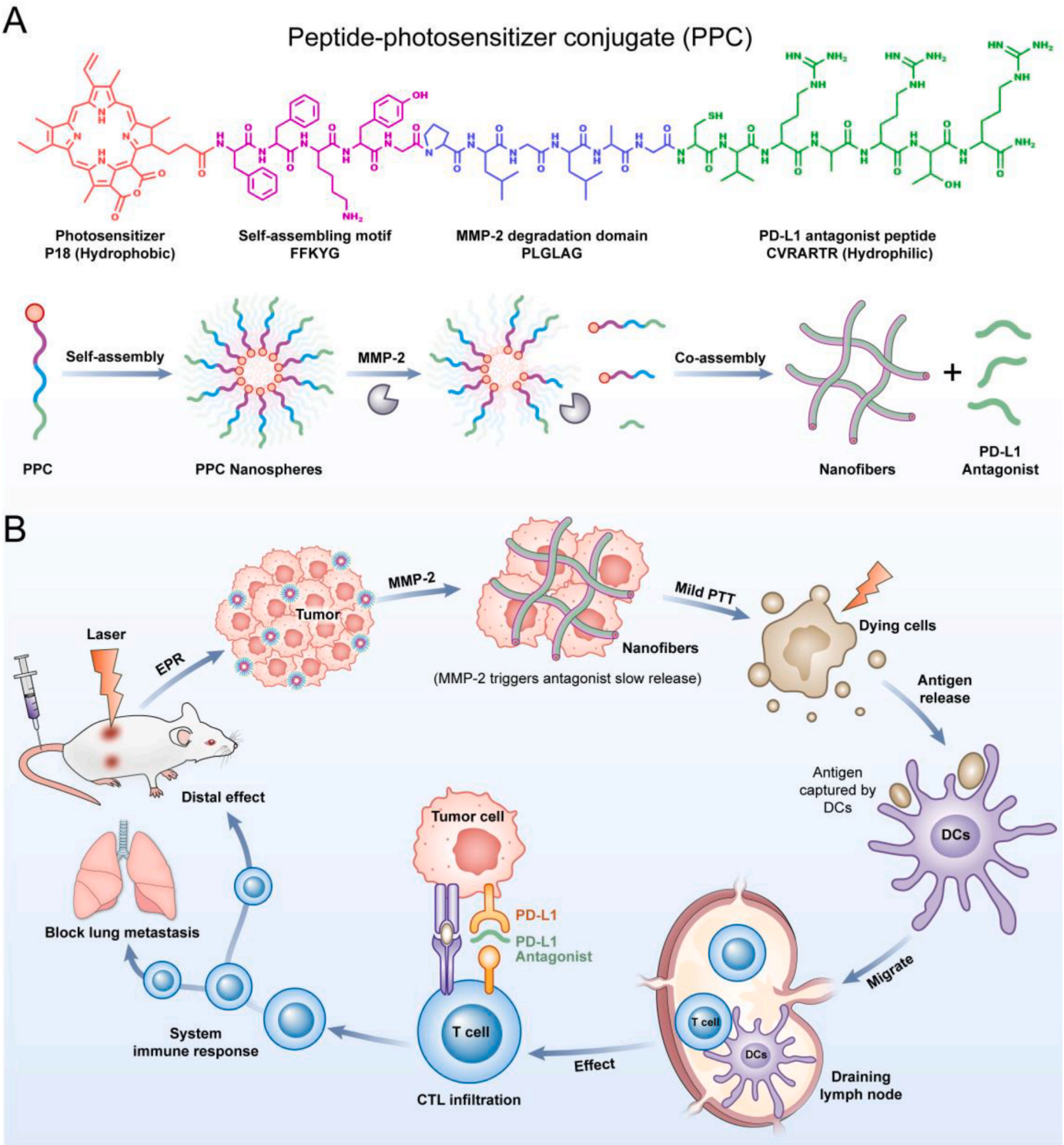

Scheme 1. Schematic illustration of MMP-2 enzyme-responsive and transformable PD-L1 blocking peptide-photosensitizer conjugate (PPC nanospheres) enables efficient PTT combined checkpoint blockade immunotherapy for breast cancer. (A) The structure and transformable ability of PPC. (B) The anti-tumor mechanism of PPC.

incapable of preventing tumor recurrence and the formation of distant metastases [21]. This situation has inspired scientists to combat refractory cancers by using photothermal immunotherapy. The combination of mild PTT and immune checkpoint inhibitors could overcome the aforementioned drawbacks of monotherapy and achieve a synergistic antitumor effect [19,22,23]. Currently, a large variety of strategies have been proposed and designed to enhance the effectiveness of combination therapies. However, many challenges remain despite remarkable progress. In some cases, the immune checkpoint-targeted antibodies are administered individually [24,25]. Other researchers prefer to integrate different therapeutic modalities into one system to achieve tumor targeting and responsive release by physically adsorbing or chemically connecting the antibodies to the carrier [26,27]. However, these strategies can either increase the uncertainty of in vitro and *in vivo* behaviors of the systems or compromise some functions of the antibody. Alternatively, the complex delivery system may limit its clinical translation and regulatory approval.

Self-assembled peptides have been widely used in disease diagnosis and drug delivery due to their multiple biological responses and good biocompatibility [28]. Peptides that contain self-assembling motifs (e.g., diphenylalanine or FFs) can assemble into highly ordered supramolecular structures in response to changes in temperature, pH, ionic strength, and enzymatic hydrolysis under conditions that are relatively moderate [29,30]. The expression and activity of some enzymes in the tumor microenvironment can be altered because of an imbalance in tumor metabolism and proliferation [31–34]. Therefore, various multifunctional peptides have been designed and constructed. Prof. Wang's group have made groundbreaking work in the field of in situ peptide self-assembly and synthesized a series of peptides with assembly induced retention (AIR) effect [35]. Upon reaching the tumor, the engineered peptides, in response to tumor-associated enzymes, can assemble into nanofibers which extends their retention time in the tumor [36]. In addition, the use of rational modular designs can offer a convenient and promising strategy to integrate multiple biological components into a single-component peptide and enable the smart delivery of the therapeutic agents [37].

This work developed a self-assembled PD-L1 blocking peptide-photosensitizer conjugate (PPC) for use in combined photothermal and immunotherapies. Compared to previously reported photothermal immunotherapy, the structure-defined PPC we constructed has multiple advantages. It overcomes the limitations of antibody, the complexity of carrier preparation, and the inconvenience of multi-component administration. The PPC consists of four components (Scheme 1A): (1) Purpurin 18 (P18), a photosensitizer that generates heat under laser irradiation; (2) FFKYG, a self-assembling motif for self-assembly of PPCs and enzymatic degradation; (3) PLGLAG, an efficient substrate for degradation by MMP-2 in the tumor microenvironment; and (4) CVRARTR, a PD-L1 antagonist peptide and an alternative to an antibody to promote ICB, which have been widely studied because of their unique advantages [38,39]. The amphiphilic peptide PPC could self-assemble into nanospheres in aqueous solution. As illustrated in Scheme 1B, PPC nanospheres passively accumulate in the tumor via the EPR effect. After reaching the tumor, the overexpressed MMP-2 gradually degrades the PPC (between PLG and LAG), releasing the PD-L1 antagonistic peptide for ICB and P18-FFKYGPLG for self-assembly. Similarly, the MMP-2 expression in tumors is enhanced due to the action of mild PTT. All these factors contribute to the co-assembly of PPC and P18-FFKYGPLG. The resulting nanofibers enhance the local retention of PPCs which promotes the slow release of antagonists and enhances PTT efficacy. The immunogenic microenvironment generated by mild PTT promotes phagocytosis of antigens by DCs and the maturation of DCs, which then migrate to the lymph nodes to activate tumor-specific cytotoxic T lymphocytes (CTLs). The combination of mild PTT and antagonistic peptides affects the local immunosuppressive tumor microenvironment and helps CTLs kill tumor cells to achieve a systemic immune effect, which may also inhibit distal tumor growth and metastasis.

2. Materials and methods

2.1. Materials

Chemicals: All 9-Fluorenylmethoxycarbonyl (Fmoc)-protected amino acids, 2-(1H-benzotriazole-1-yl)-1,1,3,3-tetramethy-luronium hexafluorophosphate (HBTU) and Rink amide-MBHA resin were purchased from GL Biochem (China). Purpurin 18 was purchased from Frontier (USA). Recombinant Human MMP-2 (cat# 10082-HNAH) was purchased from Sino Biological (China). Anti-MMP2 Antibody (cat# EPR17003) and anti-PD-L1 Antibody (cat# EPR20529) used for WB were purchased from Abcam (UK). GAPDH rabbit polyclonal antibody (cat# 37985) was purchased from SAB (USA). PE anti-mouse CD3 antibody (cat# PE-65077) was purchased from Proteintech (USA). PE anti-mouse CD274 antibody (cat# 124307), FITC anti-mouse CD8 antibody (cat# 100706), APC anti-mouse CD4 antibody (cat# 100412), FITC anti-mouse CD11c antibody (cat# 117305), PE anti-mouse CD80 antibody (cat# 104707) and APC anti-mouse CD86 antibody (cat# 105011) were purchased from BioLegend (USA). Collagenase IV, hyaluronidase and Bouin's solution were purchased from Solarbio (China). Mouse Leukocyte Isolation Kit for tumor infiltrating tissue was purchased from TBD (China). Ilomastat was purchased from TargetMol (USA). DMEM, penicillin-streptomycin liquid and trypsin were obtained from M&C Gene Technology (China). Fetal bovine serum (FBS) was purchased from Gibco (USA). All other reagents and solvents were analytical grade.

Cell culture: The mouse breast cancer cell line 4T1 cells were purchased from Chinese Academy of Medical Sciences (Beijing, China). 4T1 cells were cultured in DMEM cell culture medium supplemented with 10% FBS, 1% penicillin and 1% streptomycin cultured at 37 °C in a humidified 5% CO_2 atmosphere.

Animals: BALB/c mice (4–6 week, 18–20 g, female) were purchased from Laboratory Animal Center of Peking University Health Science Center (Beijing, China). The mice were kept in IVC mouse cages, with standard conditions (25 °C, normal humidity), and distilled water and sterilized food were available. All animal experiments were performed in Center for Experimental Animals, Peking University. All the animal experiments were executed according to the guidelines of a National Institutes of Animal Care and Use Committee and the protocol approved by the Institutional Animal Care and Use Committee of Peking University.

2.2. Synthesis and characterization of PPC

The peptides were synthesized through Fmoc solid-phase peptide synthesis method. Then purpurin 18 was dissolved in DMF and activated by DIC/OxymaPure to couple to the resin. The peptides were cleaved from the resin and precipitated in ice diethyl ether. The crude product was purified using a preparative reversed-phase high performance liquid chromatography (HPLC) (Waters, USA). The final product was acquired by freeze drying.

The product was characterized with HPLC and MALDI-TOF mass spectrometry. The purity of peptide (P18-FFKYG-PLGLAG-CVRARTR, PPC) was characterized by analytical HPLC (Agilent, USA). The mass of peptide was analyzed by MALDI-TOF mass spectrometry (AB SCIEX, USA). The purity of peptide was over 95% for the next experiments.

2.3. Preparation and characterization of PPC nanospheres

The PPC could self-assemble into nanospheres in aqueous solutions simply due to its amphiphilic property. The PPC powder was dispersed in PBS. Then, the PPC solution was managed by a supersonic cell disruptor (JY92-2D, China) for 10 min to form PPC nanospheres without the aid of additional carrier or stabilizer. The hydrodynamic diameter of

PPC nanospheres was measured by a dynamic light scattering (DLS) analysis using a Zetasizer Nano ZS (Malvern, United Kingdom). The morphology was evaluated using transmission electron microscopy (TEM) (JEM 1200EX, Japan). The ultra-violet-visible-near infrared (UV-VIS-NIR) absorption spectra of PPC nanospheres was measured by a UV spectrophotometer (Shimadzu, Japan). The fluorescence spectra of PPC nanospheres was analyzed by a fluorescence spectrophotometer (Hitachi, Japan). The secondary structures of PPC nanospheres in PBS were determined by circular dichroism (CD) spectrometer (Jasco, Japan).

The temperature variation and thermal imaging of PPC nanospheres was measured by using an FLIR camera (Fotric, USA). To measure the photothermal conversion efficiency, PPC nanospheres with a concentration of 100 μg/mL (0.2 mL) were irradiated with a 660 nm laser at 0.8 W/cm^2 for 8 min. The laser was turned off and the sample was cooled down to ambient temperature. The temperature of the sample was monitored using an infrared thermal camera. On the basis of the reported method [40], the photothermal conversion efficiencies (η) were calculated as following:

$$\eta = \frac{hS\Delta T_{max} - Q_s}{I(1 - 10^{-A_{660}})}$$

$$hS = \frac{mCwater}{\tau_s}$$

$$t = -\tau_s Ln(\theta)$$

$$\theta = \Delta T / \Delta T_{max}$$

where h is the heat transfer coefficient; S is the surface area of the container; Qs represents heat dissipated from the laser mediated by the solvent and container; I is the laser power; A is the absorbance at 660 nm; m is the mass of the solution; Cwater is the specific heat capacity of the solution; τ_s is the associated time constant; θ is a dimensionless parameter. PPC nanofibers were obtained by incubating PPC nanospheres with MMP-2 for 24 h, the photothermal conversion efficiency of PPC nanofibers was also conducted as mentioned above. To measure the photothermal stability, PPC nanospheres with a concentration of 500 μg/mL (0.2 mL) were irradiated with a 660 nm laser at 0.5 W/cm^2 for 5 min. Then the laser was turned off and the sample was cooled down to ambient temperature. The irradiation was repeated twice with the same power and method. The temperature of the sample was monitored using an infrared thermal camera. The photothermal stability of PPC nanofibers was also conducted as mentioned above.

2.4. The MMP-2 responsiveness of PPC nanospheres

MMP-2 specific cleavage was conducted by incubating PPC nanospheres (1 mM) with TCNB buffer (pH 7.4) in the presence of MMP-2 (4 μg/mL) for 24 h. PD-L1 antagonist peptide release was assayed by incubating PPC nanospheres with TCNB buffer (pH 7.4) in the presence of MMP-2 (4 μg/mL) for 4, 24, 48, 72 h. Then the reactant was analyzed by HPLC with an acetonitrile/H_2O gradient from 55% acetonitrile to 85% acetonitrile in 20 min. The mass changes were determined by MALDI-TOF mass spectrometry. The size and morphology change were evaluated using a Malvern Zetasizer Nano ZS and transmission electron microscopy. The spectral changes were determined by UV, fluorescence and circular dichromatic spectrometer, respectively.

2.5. The effect of mild PTT on 4T1 cells

The 4T1 cells were seeded in 12-well plates and incubated overnight at 37 °C. The cells were incubated with PPC nanospheres for 4 h and irradiated by a 660 nm laser for 10 min (keep the temperature for 43 °C). After incubation overnight, the cells with different treatments were lysed. The expression of MMP-2 and PD-L1 were analyzed by Western Blot according to the protocols.

2.6. In vitro cytotoxicity assay

The 4T1 cells were seeded in 96-well with 1 × 10^4 cells per well and incubated overnight. PPC nanospheres, CVRARTR (abbreviated as CVR) and LAGCVRARTR (abbreviated as LAG) antagonistic peptides with different concentrations in DMEM medium were added to the cells and incubated at 37 °C for 24 h. The cell survival rate was analyzed by CCK8 assay.

The 4T1 cells were seeded in 96-well with 1 × 10^4 cells per well and cultured overnight. The cells were replaced with cell medium containing PPC nanospheres (100 μg/mL) incubated for 4 h, then the cells were irradiated with a 660 nm laser at 0.5 W/cm^2 for 10 min. Then the cells were washed with PBS for three times and incubated with new medium overnight. The cell survival rate was analyzed by CCK8 assay.

2.7. The affinity of antagonist peptides for PD-L1 on 4T1 cells

The 4T1 cells were seeded in 6-well with 1 × 10^6 cells per well and incubated overnight. The cells were incubated with IFN-γ for 24 h to simulate the expression of PD-L1. The cells were digested with trypsin and centrifuged at 1000 rpm for 5 min, then blocked with 1% BSA at room temperature. The CVR and LAG antagonistic peptides were incubated with 4T1 cells at 50 μg/mL at 4 °C for 1 h. The cells were washed twice and suspended in 100 μL Cell Staining Buffer, and incubated with PE anti-mouse PD-L1 antibody at 4 °C for 1 h. The cells were washed twice and suspended in Cell Staining Buffer and analyzed through a flow cytometer (Calibur, BD, USA).

2.8. Shape transformation of PPC nanospheres on 4T1 cells

The 4T1 cells were seeded in cell culture dishes and incubated overnight. The cells were incubated with or without PPC nanospheres overnight. The cells were washed with PBS for twice and fixed with glutaraldehyde and then observed by scanning electron microscope (JSM-7900F, Japan).

2.9. In vivo biodistribution of PPC nanospheres

The 4T1 tumor-bearing mice were established by subcutaneous inoculation 5 × 10^5 4T1 cells in the right flank of female BALB/c mice. The mice were divided into two groups when the volume of tumor reached about 100 mm^3. 100 μL of PPC nanospheres (2.845 mg/mL) suspended in PBS solution was injected via the tail vein, and 100 μL of free P18 solution (10% DMSO in PBS solution) was used as control. The biodistribution of mice were performed using an IVIS Lumina II imaging system under isoflurane anesthesia at different points as 1 h, 3 h, 6 h, 9 h, 12 h, 24 h after the injection by observing the fluorescence of P18 [41]. The average fluorescence intensity of the tumor site in two groups was calculated. The major organs such as heart, liver, spleen, lung, kidney and tumor were imaged by this IVIS imaging system at 24 h post-injection. Further the retention ability of PPC and P18 solution were evaluated through intratumoral injection with 10 μL. The intensity of mice were performed using an IVIS Lumina II imaging system under isoflurane anesthesia at different points as 6 h, 12 h, 24 h, 48 h, 72 h, 96 h, 120 h after the injection.

To assess the influence of shape transformation on the biodistribution of PPC nanospheres, we performed two groups with or without MMP-2 inhibitor (Ilomastat). Firstly, the 4T1 tumor-bearing mice were intratumorally injected with Ilomastat at a dose of 8 mg/kg 15 min before the administration [42]. Then the two groups with or without Ilomastat injection were intratumorally injected with PPC nanospheres. The fluorescence images of the tumor were collected by this IVIS imaging system at different time points.

Bio-TEM was used to evaluate the nanofibers formation of PPC nanospheres in tumor tissues. The 4T1 tumor-bearing mice were intratumorally injected with PPC nanospheres. The mice treated with PBS

were used as control. The tumor tissues were divided into small pieces and fixed in glutaraldehyde. Then the fixed tumor tissues were made into samples and observed by TEM (JEM 1200EX, Japan).

2.10. In vivo photothermal effect

For *in vivo* photothermal effect, 4T1 tumor-bearing mice were divided into two groups. 100 μL of PPC nanospheres (2.845 mg/mL) suspended in PBS solution were injected via the tail vein, and 100 μL of free P18 solution were used as control. After 6 h of postinjection, the tumor region of these two groups were irradiated with an 660 nm laser at an suitable power density (0.5 W/cm^2) for 6 min. The photothermal image of the mice in the two groups were collected by the infrared thermal camera. The P18 group was performed as the control group which was treated in the same conditions.

2.11. In vivo anti-tumor efficacy and safety studies

The 4T1 tumor-bearing mice were established as above. When the tumor volume reached approximate 100 mm^3, the mice were randomly divided into five groups (n = 5): PBS, PPC nanospheres, PPC + NIR, P18 + CVR + NIR, CVR. The administration dosage of PPC was 2.845 mg/mL in PBS, the dosage of P18 was 0.628 mg/mL in PBS solution (10% DMSO), and the dosage of CVR was 1 mg/mL in PBS. Administration was performed on day 0 and 5, respectively. After 6 h of tail vein injection, the PPC + NIR and P18+CVR + NIR groups were irradiated with 660 nm laser for 6 min with suitable power respectively (the laser power was set as the tumor temperature of PPC group was about 45 °C). The tumor temperature change was monitored by an infrared thermal camera (FLIR Systems Inc., FOTRIC 226S). The tumor volumes and body weights of each group were recorded every two days in the following days. The tumor volume was measured and calculated by a formula: V = 1/2 × a × b^2 (a and b are the tumor length and width, respectively). After the observation, the tumor tissue was removed, weighed and photographed.

On day 16, the whole blood of five groups were collected for hematology analysis to assess white blood cells (WBC) and red blood cells (RBC) by HITACHI automatic biochemical analyzer (HITACHI, Japan). In addition, the serum samples were evaluated for the liver function and renal function of each mice. Subsequently, mice were sacrificed by cervical dislocation and major organs including heart, liver, spleen, lung, kidney were harvested and stained by a standard hematoxylin and eosin (H&E) staining protocol to observe the pathology change. The CD8 assay of immunohistochemical analysis was adopted to assess the anti-tumor efficacy of each group.

2.12. In vivo immune response and cytokines evaluation

To evaluate the immune response caused by the therapy, the primary tumors, lymph nodes, and serum were collected from mice in different groups. On day 7, the primary tumors and tumor draining lymph nodes (near the side of the tumor) were collected from mice in the five groups. For further flow cytometry analysis, tumors were divided and digested using collagenase IV and hyaluronidase at 37 °C for 2 h. Lymphocytes in tumors were obtained through Mouse Leukocyte Isolation Kit for tumor infiltrating tissue according to standard protocols. The cell suspension was filtered through a 0.22 μm filter membrane. Then the single cell suspension was incubated with PE anti-mouse CD3 Antibody and FITC anti-mouse CD8 Antibody or APC anti-mouse CD4 Antibody according to the protocols, to assess the content of CTL cells ($CD3^+CD8^+$) and $CD4^+$ T cells ($CD3^+CD4^+$) in the tumor.

For DC maturation assessment, tumor draining lymph nodes were harvested for flow cytometry analysis. The cell suspension was filtered through a 0.22 μm filter membrane after tissue grinding. Then the single cell suspension was incubated with FITC anti-mouse CD11c Antibody, PE anti-mouse CD80 Antibody and APC anti-mouse CD86 Antibody according to the protocols. The frequency of matured DCs ($CD11c^+CD80^+CD86^+$) in tumor draining lymph nodes was assessed by flow cytometry after the staining.

Serum samples were collected and analyzed for blood biochemistry from mice in the five groups on day 3 (n = 3). The content of TNF-α, IL-6, and IL-12 in the serum were detected by ELISA kits according to protocols.

2.13. In vivo distal therapeutic effects

To evaluate the distal anti-tumor effect in distal tumors, the inhibition of distal tumor growth was conducted using a 4T1 tumor-bearing mice model. The model was constructed as follows: 4T1 cells (1×10^6) were subcutaneously injected into the left flank of the mice on day −9 for the primary tumors, the distal tumors were inoculated by injecting 4T1 cells (5×10^5) in the right flank of mice on day −3. The mice were divided into five groups and were treated as described in 2.11. Administration and mild PTT were performed on day 0, 3, 6 and 9, respectively. The distal tumor volumes and body weights of each group were recorded every two days in the following days. After the observation, the lungs of each group were collected and fixed in Bouin's solution.

2.14. Statistical analysis

All values were expressed as mean ± SD (standard deviation). Statistical analysis was performed with the two-tailed Student's t-test and one-way ANOVA. P value < 0.05 was considered as the statistically significant difference between two groups in the case. Random allocation was adopted for *in vivo* experiments.

3. Results and discussion

3.1. Preparation and characterization of MMP-2 responsive PPC nanospheres

PPC peptide (Fig. S1) was synthesized using standard solid-phase peptide synthesis methods. The crude product was purified by preparative liquid chromatography after the final reaction. The purity of the target peptide was confirmed by high-performance liquid chromatography (HPLC) and matrix-assisted laser desorption/ionization-time of flight mass spectrometry (MALDI-TOF-MS). Fig. 1A shows that the PPC produced a single peak by HPLC analysis. The MALDI-TOF-MS indicated a molecular weight of 2558.3 for the PPC (Fig. S2), which is consistent with its theoretical molecular weight. PPC nanospheres were then prepared in a phosphate-buffered solution (PBS) solution using a sonication method. The PPC nanospheres had a diameter of 230.5 ± 37.05 nm as determined by dynamic light scattering. These PPC nanospheres were composed of only one component with a definite spherical structure (Fig. S3). The loading efficiency of the antagonistic peptide drug and the loading efficiency of the photosensitizer was 43% and 22%, respectively. The high drug-loading rate and the relatively simple quality control procedures were beneficial for clinical translation.

The MMP-2-responsive performance of the PPC nanospheres was assessed by numerous methods.

PPC remained 54% and produced a new chromatographic peak after incubating with MMP-2 for 24 h. The PD-L1 antagonist peptide release rate slowed down significantly from 24 h to 72 h due to the assemble of peptide (Fig. S4). This was also verified by MALDI-TOF-MS, which determined the molecular weights of PPC and its cleaved residue (Fig. 1B). These results demonstrate that PPC can be cleaved by MMP-2 to generate P18-FFKYGPLG and ICB peptide residues. The MMP-2 triggered assembly behavior of the PPC nanospheres was then assessed by dynamic light scattering and transmission electron microscopy (TEM) measurements at the same time. In addition, Fig. 1C shows that the size of the PPC nanospheres increased to ~1000 nm after MMP-2 treatment. The TEM results also demonstrated the formation of PPC nanofibers

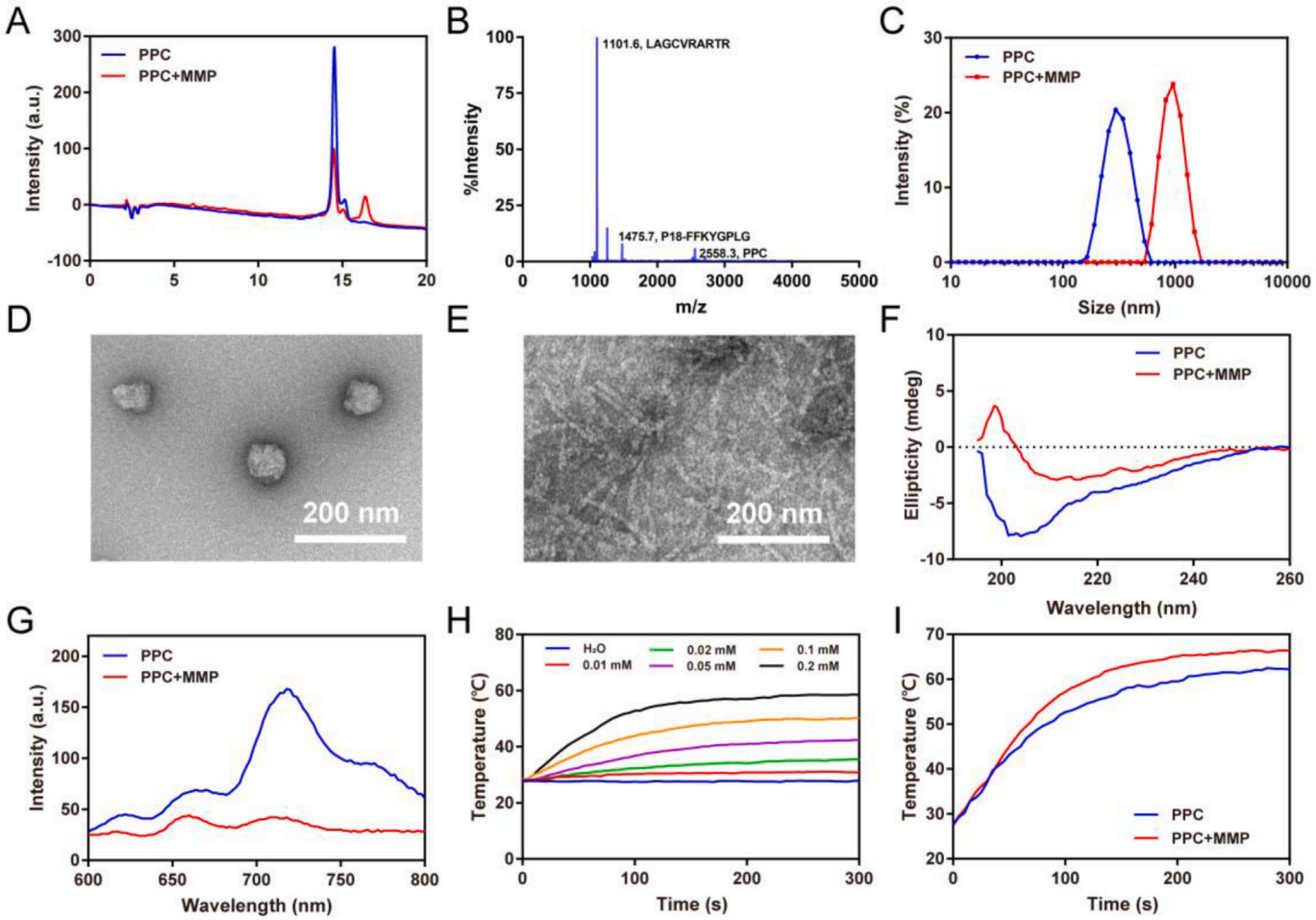

Fig. 1. Preparation and characterization of MMP-2 responsive PPC nanospheres. (A) HPLC spectrum of PPC nanospheres incubated with or without MMP-2 for 24 h. (B) MALDI-TOF mass spectrum of PPC nanospheres incubated with MMP-2 for 24 h. (C) Size distribution of PPC nanospheres incubated with or without MMP-2 for 24 h. (D) TEM image of PPC nanospheres. (E) TEM image of PPC nanospheres incubated with MMP-2 in TCNB buffer for 24 h. (F–G) CD spectra and FL spectrum of PPC nanospheres incubated with or without MMP-2 for 24 h. (H) Photothermal temperature curves of PPC nanospheres with different concentrations. (I) Photothermal temperature curves of PPC nanospheres (0.25 mM) incubated with or without MMP-2 for 24 h.

triggered by MMP-2 after incubation with MMP-2 for 24 h (Fig. 1D and E). The gradual transformation of PPC nanospheres to nanofibers could be observed from 6 h to 24 h (Fig. S5). In contrast to the aforementioned PPC nanofibers (Fig. 1E), P18-FFKYGPLG could assemble into short nanofibers after incubating overnight at 37 °C (Fig. S6). Few nanofibers were visually observed because of their low solubility in PBS. The TEM results showed the formation of PPC nanofibers after incubation with MMP-2 for 24 h and there was almost no nanoparticles (Fig. 1E). PPC couldn't present as a single molecule in the system at this concentration (~0.5 mg/mL), so PPC and their degradation products both existed in the nanofibers. Based on the aforementioned enzymatic hydrolysis experiments and the morphology of the nanofibers, it was speculated that the formed nanofibers of PPC nanospheres after MMP-2 digestion were composed of P18-FFKYGPLG and PPC. Morphological transformations occur as designed based on the aforementioned data. Thus, the shape transformation process involves co-assembly between the two building blocks, i.e., P18-FFKYGPLG and PPC. The assembly mode in the current study is similar to that described by Prof. Xu, in which partial enzymatic hydrolysis resulted in co-assembled nanofibers [43,44]. This co-assembly mechanism could occur after a portion of precursor molecules respond to enzymatic cleavage, which didn't over-depend on the high expression of the enzyme at the pathological site and improved the sensitivity of deformation response.

The MMP-2 responsive behavior of PPC nanosystems was assessed further using spectroscopic methods. The CD spectrum exhibited a negative peak at 218 nm for the PPC after incubation with MMP-2 (Fig. 1F), which is typical for a β-sheet structure [45]. The UV-VIS absorption spectrum indicated a small broad redshift after incubation with MMP-2 (Fig. S7), which was likely due to molecular aggregation [35]. The fluorescence intensity of the PPC decreased after incubation with MMP-2, due to self-quenching by molecular aggregation (Fig. 1G). Subsequently, the photothermal capability of the PPC was evaluated. Fig. 1H shows the temperature of the PPC increased with increasing concentrations following laser irradiation. After incubation with MMP-2, the PPC exhibited a remarkable increase in temperature (Fig. 1I), which was due to the lowered fluorescence yield and enhanced photothermal conversion efficiency after the formation of more dense aggregates (Fig. S8) [35,46]. PPC nanofibers showed little loss of heat-generation under the irradiation, which indicated its good photothermal stability (Fig. S9). These in vitro MMP-2 responsive release and assemble behaviors of PPC nanospheres provide a basis for further research.

3.2. *In vitro mild PTT effect and structure transformation of PPC nanospheres in 4T1 cells*

Inspired by the excellent MMP-2 responsive performance of the PPC nanospheres, their effects on 4T1 cells were then evaluated. First, the

effect of mild PTT on the expression of MMP-2 and PD-L1 toward 4T1 cells was evaluated by Western blot analysis. Figs. 2A and S10 showed that mild PTT (43–45 °C) upregulated the expression of MMP-2 and PD-L1 in 4T1 cells, which was consistent with a published report [19,47], and may be a self-protection mechanism in cell. Mild PTT can sensitize 4T1 cells to ICB treatments because of the upregulated PD-L1, which laid the foundation for the combination of mild PTT and ICB. Furthermore, the increased MMP-2 level was beneficial for the continuous release of the antagonistic peptide.

The viability of 4T1 cells treated separately with PPC, CVR (i.e., CVRARTR), and LAG (i.e., LAGCVRARTR) was then evaluated. Figs. S11–S13 show no effect on cell viability at concentrations below 200 μg/mL. Cell viability decreased when the PPC group was irradiated with a NIR laser (Fig. 2B). A Calcein-AM/PI double stain method was used to directly observe live and dead cells. Based on CCK8 cell viability assays, the PPC + NIR group (mild PTT with ICB peptide) produced a significant percentage of dead cells, which are stained red (Fig. 2D). These results confirmed the cell-killing effect of PPC.

Next, the combined effect of CVR and LAG peptides with the PD-L1 receptor was evaluated. The CVR and LAG peptides were inferred to block the binding between PD-1 and PD-L1. Therefore, the PE anti-mouse PD-L1 antibody was incubated with 4T1 cells with or without CVR (or LAG). Flow cytometry analysis indicated that the addition of ICB peptides could efficiently decrease the PE fluorescence intensity (Fig. 2C). In addition, no difference between CVR and LAG was noted, indicating that CVR and LAG had the equivalent binding ability. Furthermore, the ability of PPC to assemble on 4T1 cells was assessed. Fig. 2E shows that the scanning electron microscopy images indicated the formation of nanofibers on the surface of 4T1 cells after incubating with PPC nanospheres overnight, while no filamentous structures were noted in the control group. The results of cellular-level experiments demonstrated that PPC could co-assemble on 4T1 cells mainly because of the secretion of MMP-2 by tumor cells and the more stable thermodynamic nanofiber structure [48]. In addition, other results in the literature have shown that the formation of nanofibers on the cell surface could not only increase retention time but also affect the mass exchange between cells and the outside environment, thus selectively killing tumor cells, which was expected to further expand the application of this system [36].

3.3. *In vivo* biodistribution and mild PTT performance of PPC nanospheres

To observe the *in vivo* behaviors of PPC nanospheres, the biodistribution of PPC nanospheres in 4T1 tumor-bearing mice was first investigated using an *in vivo* fluorescence imaging system. The mice were injected intravenously with PPC nanospheres and a solution of P18 as control. Fig. 3A shows that the fluorescence signal for the P18-treated

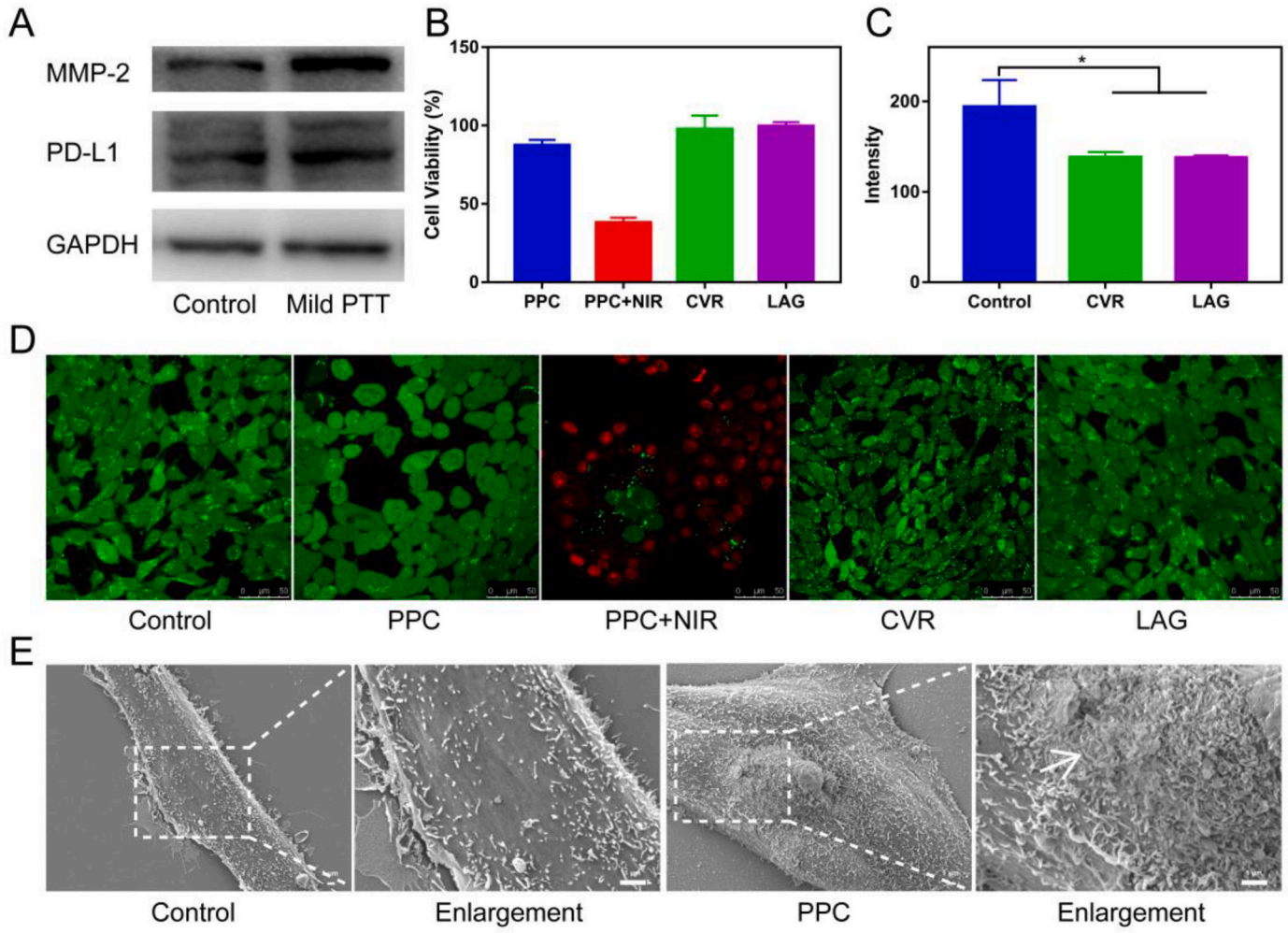

Fig. 2. In vitro mild PTT effect and structure transformable of PPC nanospheres on 4T1 cells. (A) The expression of MMP-2 and PD-L1 on 4T1 cells treated with mild PTT (measured by WB). (B) Cell viability of 4T1 cells with different groups in the same molarity conditions (PPC: 100 μg/mL , NIR: 660 nm, 10 min). (C) The PE intensity of anti-mouse PD-L1 antibody with CVR or LAG treatment measured by flow cytometry (n = 3, *p < 0.05). (D) Calcein-AM/PI double stain images of different groups. (E) SEM images of 4T1 cells incubated with or without PPC nanospheres (the arrows indicate formed nanofibers).

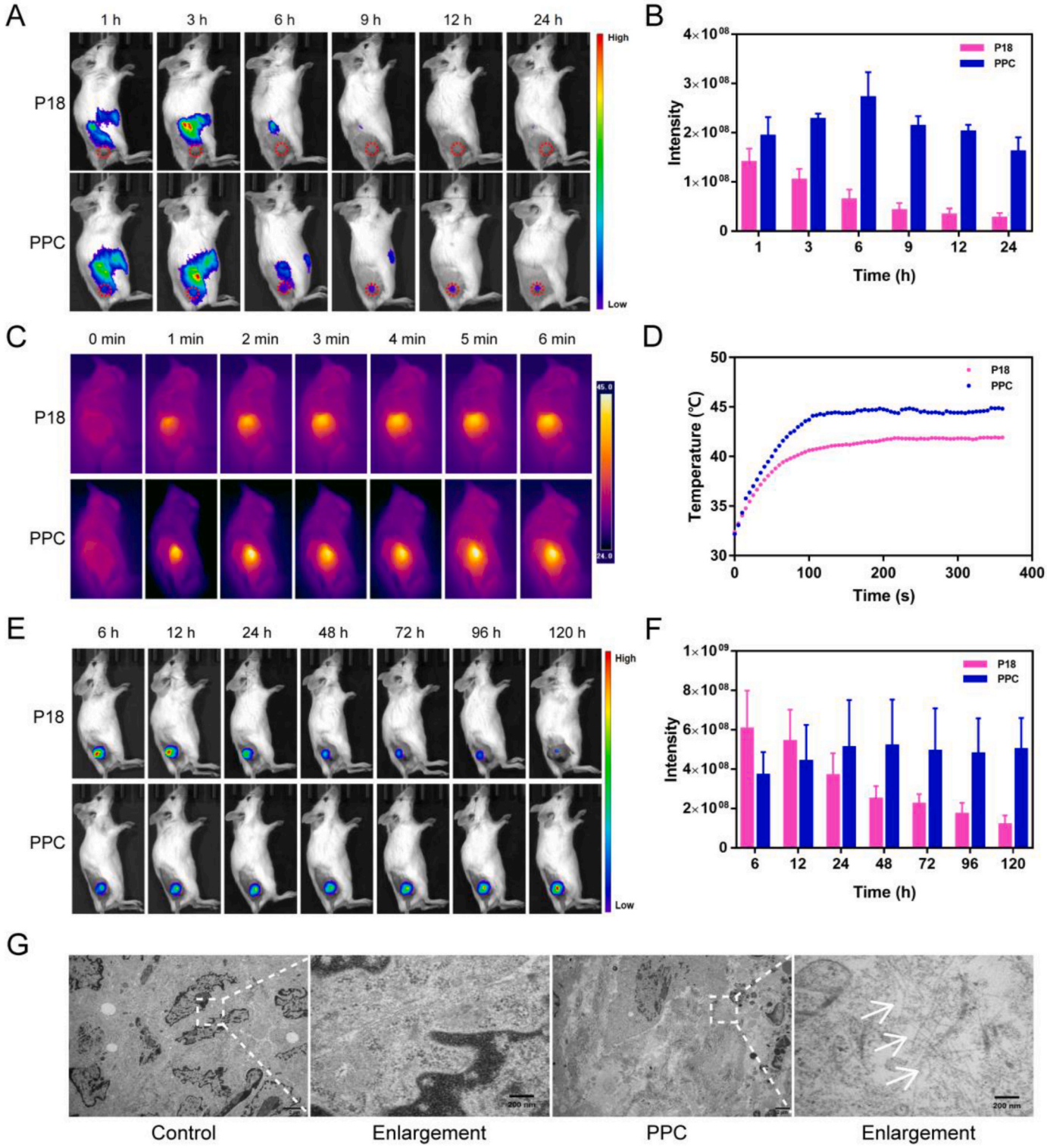

Fig. 3. Biodistribution, mild PTT performance and structure transformation of PPC nanospheres *in vivo*. (A) Fluorescence imaging of 4T1 tumor-bearing mice treated with PPC nanospheres (2.845 mg/mL) and P18 solution after tail vein injection (the dotted red circles indicate tumors). (B) Fluorescence intensity of the tumor region treated with PPC nanospheres and P18 solution during the observation. (C) Photothermal images of 4T1 tumor-bearing mice at 6 h after tail vein injection. (D) Photothermal temperature curves of the tumor region treated with PPC nanospheres and P18 solution at 6 h postinjection. (E) Fluorescence imaging of 4T1 tumor-bearing mice treated with PPC nanospheres and P18 solution via intratumoral injection. (F) Fluorescence intensity of tumor treated with PPC nanospheres and P18 solution via intratumoral injection. (G) Bio-TEM images of tumor region in 4T1 tumor-bearing mice treated with or without PPC nanospheres after 24 h (the arrows indicate nanofibers).

group was barely detectable at the tumor site. However, the fluorescence signal for the PPC group at the tumor gradually increased with time after the i.v. injection. The fluorescence intensity for the PPC group reached a peak at 6 h postinjection and maintained a strong fluorescence intensity up to 24 h or longer. The tumor fluorescence intensity was quantified to evaluate the retention of PPC nanospheres at different times. Fig. 3B shows that 60% of the peak intensity remained in the tumor at 24 h post administration. The *ex vivo* fluorescence imaging of the tumor and major organs demonstrated the tumor accumulation and retention ability of the PPC nanospheres (Fig. S14). The accumulation in lung tissue may be due to the more negatively charged amino acids of PPC. The temperature change of the tumor in 4T1 tumor-bearing mice at 6 h postinjection under laser irradiation was recorded. As shown in Fig. 3C and D, the temperature of the tumor in the PPC group reached 45 °C under laser irradiation, which was appropriate for mild PTT. The temperature of the tumor in the P18 group increased to 41 °C in response to a similar laser treatment. The temperature increase was due primarily to the higher distribution and retention of photosensitizer in the tumor.

The aforementioned results obtained after intravenous injections were due to a combination of tumor accumulation and local retention. The retention behavior was assessed separately by performing intratumoral injections (i.t.) to investigate the influence of a local enzyme response and transformation of carriers on retention. The fluorescence intensity for the P18 group decreased gradually until 120 h post i.t. injection (Fig. 3E and F). However, the fluorescence intensity for the PPC group reached peak intensity at 48 h post i.t. injection and remain at a high level during 120 h of observation (Fig. 3E and F). The results indicate that the fluorescence intensity with PPC was affected by both the molecular concentration and the degree of aggregation. Ilomastat (an inhibitor of MMP-2) was selected to assess the influence of nanofibers formation on retention in the tumor. After pre-injection of the inhibitor into the tumor, the retention time for the PPC in the tumor was significantly shortened (Fig. S15). The morphology of the PPC group at tumor sites *in vivo* was also observed by TEM. The formation of nanofibers could be observed between the tumor cells (Fig. 3G).

These findings indicate that the PPC was efficiently distributed and retained at the tumor site. The effective accumulation in the tumor was due primarily to the EPR effect caused by the PPC nanospheres, and the tumor retention benefited from the formation of nanofibers of PPC which exhibited a prolonged retention time in the tumor. In the systemic circulation, the nanospheres were more conducive to the EPR effect and were effectively distributed in the tumor. Upon reaching the tumor, the nanospheres became transformed into nanofibers in response to enzymes, achieving assembly-induced extended retention in the tumor [35,37]. After administration in the tail vein, the PPC carrier was retained in the tumor from 6 to 24 h from the transformation, and the results of intratumoral administration also indicated that it was mediated by the MMP-2 enzyme.

This study aimed to design chemically well-defined peptide conjugates to use when combining mild PTT and ICB. Immune checkpoint antagonistic peptides have great application prospects, but their half-lives *in vivo* are short. The goal of this study was to prolong the retention of peptide conjugates and ensure the responsive local release of the antagonistic peptide to produce long-lasting effects. Through the effective design of transformable peptide nanocarriers, many problems in the clinical application of immune checkpoint inhibitors can be solved (e.g., repeated administration, side effects caused by systemic administration, and poor accumulation and retention of drugs at the tumor sites). Regarding the photothermal effect, the retention of photothermal agents and the photothermal conversion efficiency could also be enhanced after forming more dense nanofiber aggregates, as discussed in the literature [35].

3.4. *In vivo anti-tumor efficacy and immune effect of PPC nanospheres*

To investigate whether the MMP-responsive nanosphere-to-nanofiber transformation could contribute to the therapeutical outcome, the combined antitumor efficacy and immune effect of PPC nanospheres in 4T1 tumor-bearing mice were evaluated. The mice were randomly divided into five groups. At 6 h postinjection, the mice in the PPC + NIR and P18 + CVR + NIR groups were irradiated with a laser for 6 min. NIR irradiation was performed on days 0 and 5 postinjection using a process that was illustrated in Fig. 4A to perform mild PTT. The PPC + NIR group (mild PTT combined immunotherapy) showed the strongest inhibition with the primary tumor (Fig. 4B), and one tumor was eradicated (Figs. S16 and S17). The PPC + NIR group (65.85 ± 49.53 mm^3) produced a minimal volume tumor on day 16 compared to the PPC (385.38 ± 118.95 mm^3), P18 + CVR + NIR (418.23 ± 30.18 mm^3), CVR (471.40 ± 114.31 mm^3), and PBS (535.19 ± 149.37 mm^3) groups. The tumor weight for the PPC + NIR group was also the most light (Fig. 4C). The temperature increase in the P18 + CVR + NIR group was slight (<42 °C) and was not enough to suppress tumor growth during the 6-min treatment. The half-life of CVR was short and was not enough to exert an antagonistic effect [39]. These findings indicate that effective distribution, adequate retention, and an appropriate mild PTT temperature (~45 °C) contributed to the enhanced inhibition of primary tumor growth.

Fig. 4D shows that the body weights of the mice among the five groups did not change during the observations. In addition, the blood cell content and blood biochemical markers for liver and kidney functions showed no differences between the five groups (Figs. S18 and S19). The H&E images of the major organs indicated no significant pathological damage (Fig. S20). These results demonstrate the excellent biocompatibility of the PPC nanospheres.

In addition, the immune effects of the PPC nanospheres during the treatment were evaluated as reported [49]. Dendritic cells play a key role in the presentation of tumor antigens and antitumor immunotherapy [50]. Therefore, whether PPC nanospheres could promote the maturation of DC cells in tumor-infiltrating lymph nodes was evaluated. On day 7, the inguinal lymph nodes of the mice were collected for flow cytometry analysis. Fig. 4E and G showed that the percentage of mature DCs ($CD11c^+CD80^+CD86^+$) in the PPC + NIR group (23.76 ± 3.01%) was significantly higher than in the other groups: PPC (19 ± 1.05%), P18 + CVR + NIR (18.2 ± 3.01%), CVR (18.9 ± 1.06%), and PBS (7.83 ± 4.33%). The presence of CTLs in the tumors of different groups was also addressed. Fig. 4F and H showed that the percentage of CTLs ($CD3^+CD8^+$) in the PPC + NIR (37.17 ± 4.52%) was greater than in the other groups: PPC (26.47 ± 4.99%), P18 + CVR + NIR (26.83 ± 5.29%), CVR (25.46 ± 5.11%), and PBS (17.07 ± 2.19%). Mild PTT released tumor antigens and DAMPs, which helped to activate the immune system [51]. In addition, the infiltration of $CD8^+$ T cells at the tumor site was evaluated by immunohistochemical analysis. Fig. S21 showed that CTLs in the tumor of different administration groups increased compared to the PBS group. There was no significant difference in the percentage of $CD4^+$ T cells in tumors (Figs. S22 and S23), which was consistent with the literature [52]. The PPC + NIR group had the largest number of $CD8^+$ cells, which was consistent with the flow cytometry results. These results demonstrate that PPC + NIR induces strong DC maturation and CTL infiltration in tumors, which can activate the immune system and suppress tumor growth.

The pro-inflammatory cytokines in the serum of mice, which included tumor necrosis factor α (TNF-α), interleukin 6 (IL-6), and interleukin 12 (IL-12), were evaluated next. TNF-α, IL-6, and IL-12 are the major biomarkers that are released by immune cells to promote the formation and activity of CTLs [19,53]. Figs. 4I, S24, and S25 showed that the levels of TNF-α, IL-6, and IL-12 in the serum, these three cytokines increased in the PPC + NIR group on day 3, which indicated the generation of a systemic immune response. Thus, benefiting from an enzyme response and a favorable nanofiber formation performance, the combination of PPC and mild PTT can promote a systemic immune response, maturation of DCs, and infiltration of CTLs in the tumor, thereby generating a powerful tumor-suppressive effect. The activation

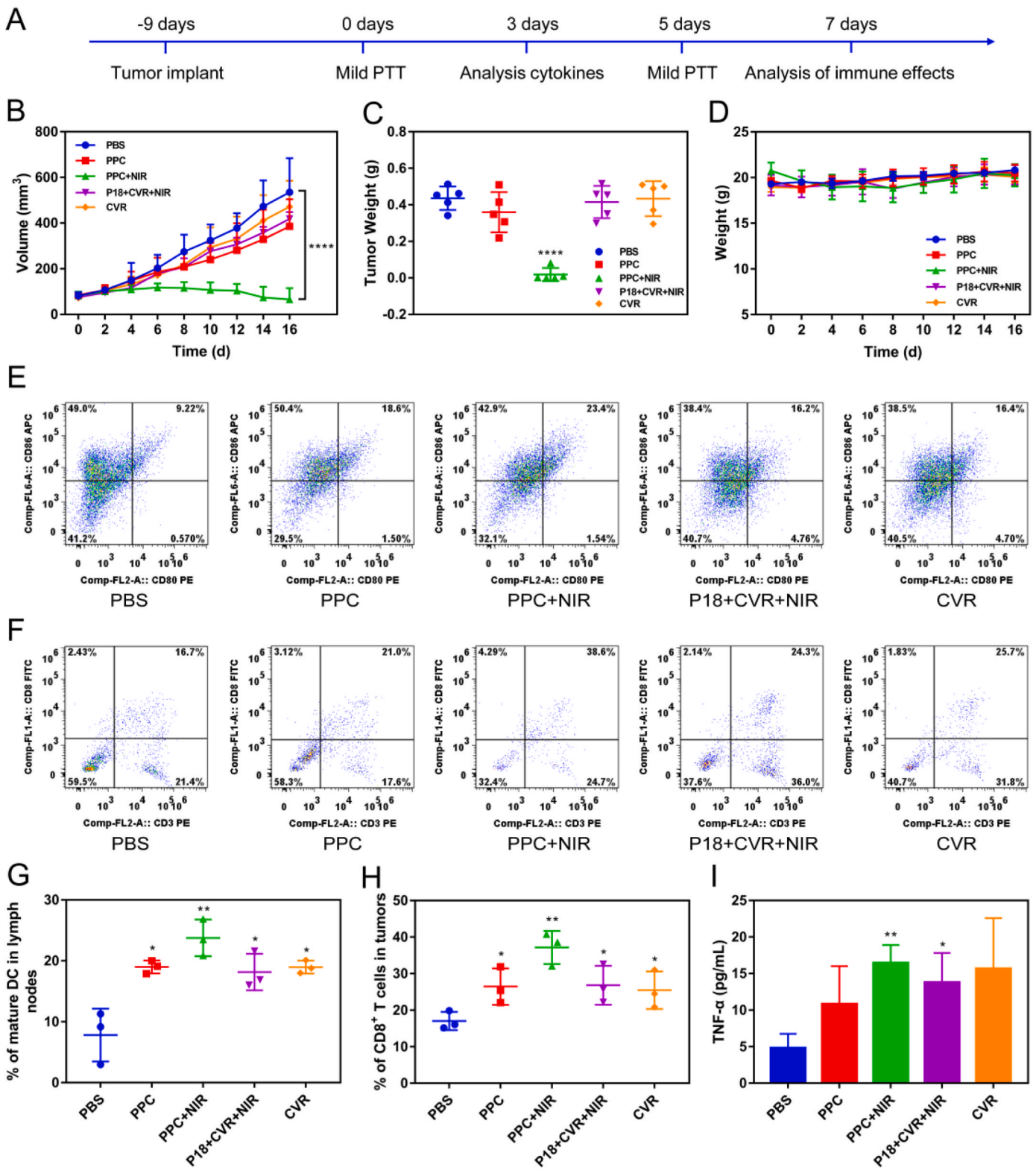

Fig. 4. *In vivo* anti-tumor efficacy and immune effect of PPC nanospheres. (A) Schematic illustration of 4T1 tumor-bearing mice experimental design. (B) Tumor volume growth curves of 4T1 tumor-bearing mice with different groups (n = 5, ****p < 0.0001). (C) Tumor weights of different groups after the treatment, significant differences were analyzed by comparing the different groups with the PBS group (n = 5, ****p < 0.0001). (D) Body weight changes of 4T1 tumor-bearing mice after different treatments (n = 5). (E, G) DCs maturation with different treatments on 4T1 tumor-bearing mice ($CD11c^+$, $CD80^+$ and $CD86^+$). Cells in the lymph nodes were collected on day 7 by flow cytometry. Data was presented by mean ± SD, significant differences were analyzed by comparing the different groups with the PBS group (n = 3, *p < 0.05, **p < 0.01). (F, H) Intratumor CTLs infiltration with different treatments on 4T1 tumor-bearing mice ($CD3^+$, $CD8^+$). Cells in tumors were collected on day 7 by flow cytometry. Data was presented by mean ± SD, significant differences were analyzed by comparing the different groups with the PBS group (n = 3, *p < 0.05, **p < 0.01). (I) TNF-α in serum of 4T1 tumor-bearing mice with different groups after 3 days, significant differences were analyzed by comparing the different groups with the PBS group (n = 3, *p < 0.05, **p < 0.01).

of a systemic immune response may also lead to a distal therapeutic effect.

3.5. *In vivo* distal therapeutic effects of PPC nanospheres

As aforementioned, the PTT-linked combination therapy in the current study induced a strong immune response. To determine if it produces a systemic antitumor effect, a distal tumor model was constructed and the inhibitory effect of the PPC on an untreated distal tumor was studied. Briefly, 4T1 cells were first implanted in the right flank of mice to simulate a primary tumor, and a distant tumor was implanted in the opposite left flank to simulate a metastatic tumor. Fig. 5A showed that treatments were administered on days 0, 3, 6, and 9. After treatment on primary tumors, the growth trend of the primary tumor was consistent with the previous study and demonstrated the design efficacy on the primary tumor. Regarding the growth of the distal tumors, as expected, the PPC + NIR group (49.82 ± 61.28 mm^3) effectively inhibited tumor growth, and the tumor in one mouse was eliminated, which was consistent with the foregoing immune effects (Fig. 5B). The PPC group (230.28 ± 46.61 mm^3) had a strong distal tumor suppression effect, which was significantly different from the PBS group (402.01 ± 53.08 mm^3). The distal tumor volume of the P18 + CVR + NIR group (342.02 ± 108.27 mm^3) was similar to the CVR group (341.65 ± 98.89 mm^3), and no significant difference was noted between these two groups and the PBS group. Because of the relatively short half-lives of peptides *in vivo*, the antagonistic effect of the antagonistic peptides (CVR) was insufficient to suppress tumor growth effectively when administered every 3 days (days 0, 3, 6, and 9) [39]. PPC + NIR induced a strong systemic immune response, which resulted in an effective distal antitumor effect.

As expected, the weights of the distal tumors in the PPC + NIR group were the lowest compared with the other four groups (Fig. 5C). The tumor images also confirmed the powerful suppressive effect in the PPC + NIR group (Fig. S26). Fig. 5D showed no significant difference in body weights among all groups, indicating good biocompatibility. In addition, the lungs in each group were examined for the presence of metastases on day 24. Fig. 5F showed that many metastatic foci in the lungs were found in these groups. In addition, the weights of the lungs increased in all groups due to tumor metastases and invasion, and the weights of the lungs were the lowest in the PPC + NIR group (Fig. 5E). These results demonstrate the excellent performance of PPC nanospheres combined with mild PTT in inhibiting lung metastasis. Finally, laser-irradiated PPCs suppressed the growth of both the primary and distal tumors and inhibited the formation of pulmonary metastases by inducing a strong antitumor system immune response.

4. Conclusions

In summary, a peptide conjugate was designed to integrate mild photothermal therapy and immunotherapy into one single-component nanosystem for breast cancer treatment. The PPCs self-assemble into nanospheres in aqueous solutions in the absence of additional excipients. The well-defined chemical components and the facile preparation process meet the fundamental prerequisites for the successful clinical

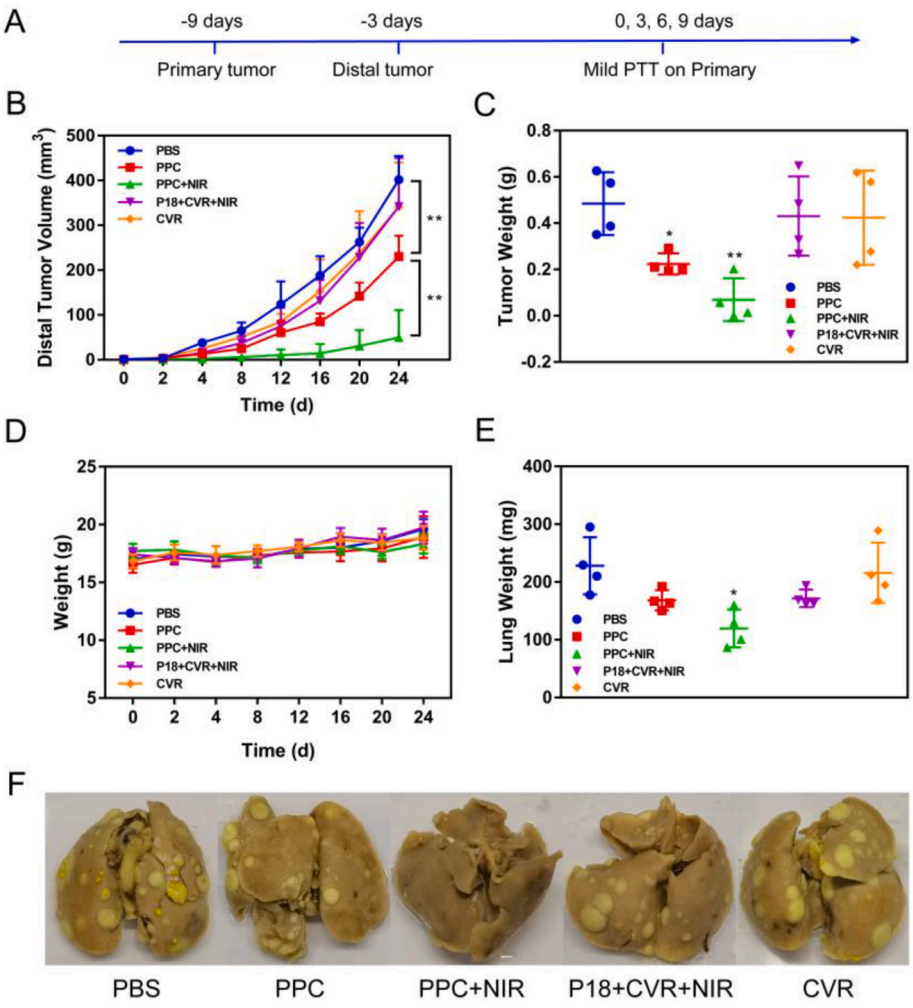

Fig. 5. *In vivo* distal therapeutic effects of PPC nanospheres. (A) Schematic illustration of 4T1 tumor-bearing mice design for distal experiment. (B) Distal tumor volume growth curves of 4T1 tumor-bearing mice with different groups (n = 4, **p < 0.01). (C) Distal tumor weights of different groups after the treatment, significant differences were analyzed by comparing the different groups with the PBS group (n = 4, *p < 0.05, **p < 0.01). (D) Body weight changes of 4T1 tumor-bearing mice after different treatments (n = 4). (E) The weight of lung tissues of each group after the observation, significant differences were analyzed by comparing the different groups with the PBS group (n = 4, *p < 0.05). (F) The representative lung tissues photographs of metastasis with different treatments.

translation of such multifunctional therapies. The unique property of the PPC nanospheres is the MMP-responsive release of PD-L1 antagonist peptide and the co-assembled induced morphology transformation, which have been characterized in vitro and *in vivo*. Consequently, the PPC nanospheres show excellent antitumor efficacy under laser irradiation, which effectively suppresses the growth of in situ tumors, distal tumors, and lung metastases *in vivo*. The PPC is composed of exchangeable modules, and this permits fine-tuning of the responsiveness, the release kinetics of immune checkpoint antagonists, and an aggregated state of photosensitizer for use in other applications. The current study provides a generalizable, tunable, and simple strategy for combinational photoimmunotherapy for diverse cancers that are refractory to ICB as well as mild PTT.

Ethics approval and consent to participate

All animal experiments were performed in Center for Experimental Animals, Peking University. All the animal experiments were executed according to the guidelines of a National Institutes of Animal Care and Use Committee and the experimental protocol was approved by the Institutional Animal Care and Use Committee of Peking University.

CRediT authorship contribution statement

Yanan Sun: Term, Conceptualization, Methodology, Investigation, Writing – original draft, Writing – review & editing, Funding acquisition. **Bochen Lyu:** Methodology, Investigation. **Chang Yang:** Supplement experiment, Investigation. **Bing He:** Validation. **Hua Zhang:** Validation. **Xueqing Wang:** Validation. **Qiang Zhang:** Writing – review & editing, Funding acquisition. **Wenbing Dai:** Writing – review & editing, Supervision, Project administration, Funding acquisition.

Declaration of competing interest

The authors declare no conflict of interest.

Acknowledgments

This work was supported by the National Key R&D Program of China (2017YFA0205600), Natural Science Foundation of Hebei Province (H2022206171). Wenbing Dai gratefully acknowledges Prof. Honggang Cui at Johns Hopkins University for bringing him into the field of peptide self-assembly. We are very grateful to Xiaoli Shi (Beijing Nonc Biotech Co., LTD) for helping with animal experiments.

Appendix A. Supplementary data

Supplementary data to this article can be found online at https://doi.org/10.1016/j.bioactmat.2022.08.020.

References

[1] H. Sung, J. Ferlay, R.L. Siegel, M. Laversanne, I. Soerjomataram, A. Jemal, F. Bray, Global cancer statistics 2020: GLOBOCAN estimates of incidence and mortality worldwide for 36 cancers in 185 countries, Ca - Cancer J. Clin. 71 (3) (2021) 209–249.
[2] G. Bianchini, J.M. Balko, I.A. Mayer, M.E. Sanders, L. Gianni, Triple-negative breast cancer: challenges and opportunities of a heterogeneous disease, Nat. Rev. Clin. Oncol. 13 (11) (2016) 674–690.
[3] F. Meric-Bernstam, J. Larkin, J. Tabernero, C. Bonini, Enhancing anti-tumour efficacy with immunotherapy combinations, Lancet 397 (10278) (2021) 1010–1022.
[4] A. Ribas, J.D. Wolchok, Cancer immunotherapy using checkpoint blockade, Science 359 (6382) (2018) 1350–1355.
[5] L. Wein, S.J. Luen, P. Savas, R. Salgado, S. Loi, Checkpoint blockade in the treatment of breast cancer: current status and future directions, Br. J. Cancer 119 (1) (2018) 4–11.
[6] A.J. Korman, S.C. Garrett-Thomson, N. Lonberg, The foundations of immune checkpoint blockade and the ipilimumab approval decennial, Nat. Rev. Drug Discov. 21 (7) (2022) 509–528.
[7] F.J. Esteva, V.M. Hubbard-Lucey, J. Tang, L. Pusztai, Immunotherapy and targeted therapy combinations in metastatic breast cancer, Lancet Oncol. 20 (3) (2019) e175–e186.
[8] Q. Chen, J. Chen, Z. Yang, J. Xu, L. Xu, C. Liang, X. Han, Z. Liu, Nanoparticle-enhanced radiotherapy to trigger robust cancer immunotherapy, Adv. Mater. 31 (10) (2019), e1802228.
[9] W. Yue, L. Chen, L. Yu, B. Zhou, H. Yin, W. Ren, C. Liu, L. Guo, Y. Zhang, L. Sun, K. Zhang, H. Xu, Y. Chen, Checkpoint blockade and nanosonosensitizer-augmented noninvasive sonodynamic therapy combination reduces tumour growth and metastases in mice, Nat. Commun. 10 (1) (2019), 2025.
[10] J. Choi, M.K. Shim, S. Yang, H.S. Hwang, H. Cho, J. Kim, W.S. Yun, Y. Moon, J. Kim, H.Y. Yoon, K. Kim, Visible-light-triggered prodrug nanoparticles combine chemotherapy and photodynamic therapy to potentiate checkpoint blockade cancer immunotherapy, ACS Nano 15 (7) (2021) 12086–12098.
[11] R. Vazquez-Lombardi, D. Nevoltris, A. Luthra, P. Schofield, C. Zimmermann, D. Christ, Transient expression of human antibodies in mammalian cells, Nat. Protoc. 13 (1) (2018) 99–117.
[12] M.A. Postow, R. Sidlow, M.D. Hellmann, Immune-related adverse events associated with immune checkpoint blockade, N. Engl. J. Med. 378 (2) (2018) 158–168.
[13] F. Ding, X. Gao, X. Huang, H. Ge, M. Xie, J. Qian, J. Song, Y. Li, X. Zhu, C. Zhang, Polydopamine-coated nucleic acid nanogel for siRNA-mediated low-temperature photothermal therapy, Biomaterials 245 (2020), 119976.
[14] X. Cheng, R. Sun, L. Yin, Z. Chai, H. Shi, M. Gao, Light-triggered assembly of gold nanoparticles for photothermal therapy and photoacoustic imaging of tumors in vivo, Adv. Mater. 29 (6) (2017), 1604894.
[15] M. Chang, Z. Hou, M. Wang, C. Li, J. Lin, Recent advances in hyperthermia therapy-based synergistic immunotherapy, Adv. Mater. 33 (4) (2021), e2004788.
[16] M. Li, S. Li, H. Zhou, X. Tang, Y. Wu, W. Jiang, Z. Tian, X. Zhou, X. Yang, Y. Wang, Chemotaxis-driven delivery of nano-pathogenoids for complete eradication of tumors post-phototherapy, Nat. Commun. 11 (1) (2020) 1126.
[17] J. Nam, S. Son, L.J. Ochyl, R. Kuai, A. Schwendeman, J.J. Moon, Chemo-photothermal therapy combination elicits anti-tumor immunity against advanced metastatic cancer, Nat. Commun. 9 (1) (2018) 1074.
[18] S.S. Evans, E.A. Repasky, D.T. Fisher, Fever and the thermal regulation of immunity: the immune system feels the heat, Nat. Rev. Immunol. 15 (6) (2015) 335–349.
[19] L. Huang, Y. Li, Y. Du, Y. Zhang, X. Wang, Y. Ding, X. Yang, F. Meng, J. Tu, L. Luo, C. Sun, Mild photothermal therapy potentiates anti-PD-L1 treatment for immunologically cold tumors via an all-in-one and all-in-control strategy, Nat. Commun. 10 (1) (2019) 4871.
[20] Y. Yang, W. Zhu, Z. Dong, Y. Chao, L. Xu, M. Chen, Z. Liu, 1D coordination polymer nanofibers for low-temperature photothermal therapy, Adv. Mater. 29 (40) (2017), 1703588.
[21] P.M. Chen, W.Y. Pan, C.Y. Wu, C.Y. Yeh, C. Korupalli, P.K. Luo, C.J. Chou, W. T. Chia, H.W. Sung, Modulation of tumor microenvironment using a TLR-7/8 agonist-loaded nanoparticle system that exerts low-temperature hyperthermia and immunotherapy for in situ cancer vaccination, Biomaterials 230 (2020), 119629.
[22] X. Ye, X. Liang, Q. Chen, Q. Miao, X. Chen, X. Zhang, L. Mei, Surgical tumor-derived personalized photothermal vaccine formulation for cancer immunotherapy, ACS Nano 13 (3) (2019) 2956–2968.
[23] Q. Chen, L. Xu, C. Liang, C. Wang, R. Peng, Z. Liu, Photothermal therapy with immune-adjuvant nanoparticles together with checkpoint blockade for effective cancer immunotherapy, Nat. Commun. 7 (2016), 13193.
[24] S. Bai, Z. Lu, Y. Jiang, X. Shi, D. Xu, Y. Shi, G. Lin, C. Liu, Y. Zhang, G. Liu, Nanotransferrin-based programmable catalysis mediates three-pronged induction of oxidative stress to enhance cancer immunotherapy, ACS Nano 16 (1) (2022) 997–1012.
[25] G. Wang, L. Xie, B. Li, W. Sang, J. Yan, J. Li, H. Tian, W. Li, Z. Zhang, Y. Tian, Y. Dai, A nanounit strategy reverses immune suppression of exosomal PD-L1 and is associated with enhanced ferroptosis, Nat. Commun. 12 (1) (2021) 5733.
[26] Q. Li, D. Zhang, J. Zhang, Y. Jiang, A. Song, Z. Li, Y. Luan, A three-in-one immunotherapy nanoweapon via cascade-amplifying cancer-immunity cycle against tumor metastasis, relapse, and postsurgical regrowth, Nano Lett. 19 (9) (2019) 6647–6657.
[27] Z. Gu, Q. Wang, Y. Shi, Y. Huang, J. Zhang, X. Zhang, G. Lin, Nanotechnology-mediated immunochemotherapy combined with docetaxel and PD-L1 antibody increase therapeutic effects and decrease systemic toxicity, J. Contr. Release 286 (2018) 369–380.
[28] S. Mondal, S. Das, A.K. Nandi, A review on recent advances in polymer and peptide hydrogels, Soft Matter 16 (6) (2020) 1404–1454.
[29] H. Wang, Z. Feng, B. Xu, Assemblies of peptides in a complex environment and their applications, Angew Chem. Int. Ed. Engl. 58 (31) (2019) 10423–10432.
[30] L. Yang, R. Peltier, M. Zhang, D. Song, H. Huang, G. Chen, Y. Chen, F. Zhou, Q. Hao, L. Bian, M.L. He, Z. Wang, Y. Hu, H. Sun, Desuccinylation-triggered peptide self-assembly: live cell imaging of SIRT5 activity and mitochondrial activity modulation, J. Am. Chem. Soc. 142 (42) (2020) 18150–18159.
[31] J. Westermarck, V.M. Kahari, Regulation of matrix metalloproteinase expression in tumor invasion, Faseb. J. 13 (8) (1999) 781–792.
[32] M. Liu, H. Du, W. Zhang, G. Zhai, Internal stimuli-responsive nanocarriers for drug delivery: design strategies and applications, Mater. Sci. Eng. C Mater. Biol. Appl. 71 (2017) 1267–1280.
[33] M. Liu, A.R. Khan, J. Ji, G. Lin, X. Zhao, G. Zhai, Crosslinked self-assembled nanoparticles for chemo-sonodynamic combination therapy favoring antitumor, antimetastasis management and immune responses, J. Contr. Release 290 (2018) 150–164.

[34] M. Liu, H. Du, A.R. Khan, J. Ji, A. Yu, G. Zhai, Redox/enzyme sensitive chondroitin sulfate-based self-assembled nanoparticles loading docetaxel for the inhibition of metastasis and growth of melanoma, Carbohydr. Polym. 184 (2018) 82–93.
[35] D. Zhang, G.B. Qi, Y.X. Zhao, S.L. Qiao, C. Yang, H. Wang, In situ formation of nanofibers from purpurin18-peptide conjugates and the assembly induced retention effect in tumor sites, Adv. Mater. 27 (40) (2015) 6125–6130.
[36] C. Zhang, L.H. Liu, W.X. Qiu, Y.H. Zhang, W. Song, L. Zhang, S.B. Wang, X. Z. Zhang, A transformable chimeric peptide for cell encapsulation to overcome multidrug resistance, Small 14 (11) (2018), e1703321.
[37] B. Sun, R. Chang, S. Cao, C. Yuan, L. Zhao, H. Yang, J. Li, X. Yan, J.C.M. van Hest, Acid-activatable transmorphic peptide-based nanomaterials for photodynamic therapy, Angew Chem. Int. Ed. Engl. 59 (46) (2020) 20582–20588.
[38] H.N. Chang, B.Y. Liu, Y.K. Qi, Y. Zhou, Y.P. Chen, K.M. Pan, W.W. Li, X.M. Zhou, W.W. Ma, C.Y. Fu, Y.M. Qi, L. Liu, Y.F. Gao, Blocking of the PD-1/PD-L1 interaction by a D-peptide antagonist for cancer immunotherapy, Angew Chem. Int. Ed. Engl. 54 (40) (2015) 11760–11764.
[39] S. Gurung, F. Khan, G.R. Gunassekaran, J.D. Yoo, S.M. Poongkavithai Vadevoo, U. Permpoon, S.H. Kim, H.J. Kim, I.S. Kim, H. Han, J.H. Park, S. Kim, B. Lee, Phage display-identified PD-L1-binding peptides reinvigorate T-cell activity and inhibit tumor progression, Biomaterials 247 (2020), 119984.
[40] Y. Liu, K. Ai, J. Liu, M. Deng, Y. He, L. Lu, Dopamine-melanin colloidal nanospheres: an efficient near-infrared photothermal therapeutic agent for in vivo cancer therapy, Adv. Mater. 25 (9) (2013) 1353–1359.
[41] Y. Sun, Y. Zhang, Y. Gao, P. Wang, G. He, N.T. Blum, J. Lin, Q. Liu, X. Wang, P. Huang, Six birds with one stone: versatile nanoporphyrin for single-laser-triggered synergistic phototheranostics and robust immune activation, Adv. Mater. 32 (48) (2020), e2004481.
[42] C.V. Gringeri, V. Menchise, S. Rizzitelli, E. Cittadino, V. Catanzaro, G. Dati, L. Chaabane, G. Digilio, S. Aime, Novel Gd(III)-based probes for MR molecular imaging of matrix metalloproteinases, Contrast Media Mol. Imaging 7 (2) (2012) 175–184.
[43] Z. Feng, H. Wang, B. Xu, Instructed assembly of peptides for intracellular enzyme sequestration, J. Am. Chem. Soc. 140 (48) (2018) 16433–16437.
[44] H. Wang, Z. Feng, B. Xu, Intercellular instructed-assembly mimics protein dynamics to induce cell spheroids, J. Am. Chem. Soc. 141 (18) (2019) 7271–7274.
[45] Y. Shi, P.A. Summers, M.K. Kuimova, H.S. Azevedo, Unravelling the enzymatic degradation mechanism of supramolecular peptide nanofibers and its correlation with their internal viscosity, Nano Lett. 20 (10) (2020) 7375–7381.
[46] R. Zheng, J. Yang, M. Mamuti, D.Y. Hou, H.W. An, Y. Zhao, H. Wang, Controllable self-assembly of peptide-cyanine conjugates in vivo as fine-tunable theranostics, Angew Chem. Int. Ed. Engl. 60 (14) (2021) 7809–7819.
[47] Q. Yang, J. Peng, K. Shi, Y. Xiao, Q. Liu, R. Han, X. Wei, Z. Qian, Rationally designed peptide-conjugated gold/platinum nanosystem with active tumor-targeting for enhancing tumor photothermal-immunotherapy, J. Contr. Release 308 (2019) 29–43.
[48] L. Zhang, D. Jing, N. Jiang, T. Rojalin, C.M. Baehr, D. Zhang, W. Xiao, Y. Wu, Z. Cong, J.J. Li, Y. Li, L. Wang, K.S. Lam, Transformable peptide nanoparticles arrest HER2 signalling and cause cancer cell death in vivo, Nat. Nanotechnol. 15 (2) (2020) 145–153.
[49] H. Xu, M. Hu, M. Liu, S. An, K. Guan, M. Wang, L. Li, J. Zhang, J. Li, L. Huang, Nano-puerarin regulates tumor microenvironment and facilitates chemo- and immunotherapy in murine triple negative breast cancer model, Biomaterials 235 (2020), 119769.
[50] Y. Zhai, J. Wang, T. Lang, Y. Kong, R. Rong, Y. Cai, W. Ran, F. Xiong, C. Zheng, Y. Wang, Y. Yu, H.H. Zhu, P. Zhang, Y. Li, T lymphocyte membrane-decorated epigenetic nanoinducer of interferons for cancer immunotherapy, Nat. Nanotechnol. 16 (11) (2021) 1271–1280.
[51] K.F. Chu, D.E. Dupuy, Thermal ablation of tumours: biological mechanisms and advances in therapy, Nat. Rev. Cancer 14 (3) (2014) 199–208.
[52] T. Wang, Z. He, C.S. Yuan, Z.W. Deng, F. Li, X.G. Chen, Y. Liu, MMP-responsive transformation nanomaterials with IAP antagonist to boost immune checkpoint therapy, J. Contr. Release 343 (2022) 765–776.
[53] I. Noh, Y. Son, W. Jung, M. Kim, D. Kim, H. Shin, Y.C. Kim, S. Jon, Targeting the tumor microenvironment with amphiphilic near-infrared cyanine nanoparticles for potentiated photothermal immunotherapy, Biomaterials 275 (2021), 120926.